Compression behavior of dense H_2-He mixtures up to 160 GPa

Jinhyuk Lim,[1] Minseob Kim,[1] Sakun Duwal,[1,*] Saori Kawaguchi,[2] Yasuo Ohishi,[2] Hanns-Peter Liermann,[3] Rostislav Hrubiak,[4] John S. Tse,[5] and Choong-Shik Yoo[1]

[1]*Department of Chemistry and Institute for Shock Physics, Washington State University, Pullman, Washington 99164, USA*
[2]*Materials Science Division, Japan Synchrotron Radiation Research Institute (JASRI), SPring-8, Sayo, Hyogo 679-5198, Japan*
[3]*Photon Sciences, Deutsches Elektronen-Synchrotron (DESY), Notkestraße 85, 22607 Hamburg, Germany*
[4]*HPCAT, X-ray Science Division, Argonne National Laboratory, 9700 South Case Avenue, Lemont, Illinois 60439, USA*
[5]*Department of Physics and Engineering Physics, University of Saskatchewan, Saskatoon, Canada S7N 5E2*

(Received 10 February 2020; revised manuscript received 18 April 2020; accepted 28 April 2020; published 1 June 2020)

We have studied the compression behavior of H_2-He mixtures in comparison with pure H_2 and He using powder synchrotron x-ray diffraction, and we present the pressure-volume (PV) compression data of H_2-He mixtures to 160 GPa. The results indicate that both H_2 and He in H_2-He mixtures remain in hcp to the maximum pressure studied, yet they develop a substantial level of lattice distortion in the (100) plane, most profound in He-rich solids and below 66 GPa. The measured PV data also indicate the softening of an He (or H_2) -rich lattice upon increasing the level of the guest H_2 (or He) concentration. We suggest that the observed softening and lattice distortion are due to a substitutional incorporation of H_2 (guest) molecules into the basal plane of the hcp-He (host) lattice, and thereby reflect the miscibility between H_2 and He in H_2-He mixtures. Interestingly, solid He exhibits a lesser degree of preferred orientation in H_2-He mixtures than in pure He, likely due to the presence of solid H_2 disturbing the crystalline ordering of He-rich solids. Finally, the present PV compression data of H_2-rich and He-rich solids to 160 GPa deviate from those of pure H_2 and pure He above ~70 and 45 GPa respectively, providing new constraints for the development of the equation of state for H_2-He mixtures for planetary models.

DOI: 10.1103/PhysRevB.101.224103

I. INTRODUCTION

Hydrogen and helium are two of the most fundamental quantum solids in which the atomic motions are restless even in the ground state at absolute 0 K [1]. Because of the quantum nature, recent theory predicts novel states of dense H_2 such as metallic superfluid and superconducting superfluid [2]. Hydrogen and helium are also known as two of the most abundant materials in the Universe, filling ~74% and 24% of all observable mass, respectively [3]. Giant planets such as Jupiter and Saturn are mainly composed of H_2 and He distributed into the upper molecular layer and the lower metallic layer [4]. The pressure and temperature (PT) conditions of Jupiter (Saturn), for example, span from ~200 GPa–6500 K (~200 GPa–6000 K for Saturn) at the bottom of molecular layer to ~4000 GPa–20 000 K (~1000 GPa–10 000 K for Saturn) at the bottom of the lower metallic layer [5]. Therefore, an accurate equation of state (EOS) of H_2-He mixtures is critical to develop/validate new condensed-matter theory and model the composition and structure of Giant planets.

H_2 and He crystallize into hexagonal-close-packed (hcp) structures with the same space group $P6_3/mmc$, respectively, at 5.4 and 11.5 GPa at room temperature [6,7]. Despite the extremely low x-ray diffraction (XRD) intensity of solid H_2, Mao *et al.* [6] were able to show that solid H_2 remains in hcp to 26.5 GPa by performing single-crystal XRD experiments. With considerable development in growing high-quality single-crystal H_2 in hydrostatic He, Loubeyre *et al.* [8] were able to obtain accurate EOS data of H_2 to 109 GPa. These data were based on the pressure dependence of (100), (002), and (101) peaks of H_2 single crystal, which also revealed evidence for enhanced anisotropy at high pressures. Recently, Ji *et al.* [9] successfully extended the EOS data of single crystal H_2 to 254 GPa and found two isostructural electronic transitions from phase I to phase III and IV. This study utilizes a composite gasket (Re outside and MgO/epoxy composite inside) to obtain a clean XRD background. Akahama *et al.* [10] performed low-temperature (100 K) powder XRD to 183 GPa and showed that H_2 undergoes an isostructural phase transition to phase III with ordered H_2 molecules parallel to the *ab* plane.

Mao *et al.* [7] performed single-crystal XRD on He and found that hcp He is stable up to ~23 GPa at 300 K, shortly followed by Loubeyre *et al.* [11], who extended it to 58 GPa. The high stability of hcp He observed over a large pressure range is, however, in contrast to the theoretically predicted ground state of fcc in He [12] and other rare-gas solids (RGS).

Despite the strong implications for Giant planetary models, the compression behavior and EOS of H_2-He mixtures have not been measured over the relevant PT and composition. Several theoretical calculations along with a few experiments on the mixtures [13] have focused on demixing of He-H_2 in high PT conditions relevant to the Giant planets [14,15]. Because of high temperatures, these calculations have not taken into

[*]Present address: Sandia National Laboratories, P.O. Box 5800, Albuquerque, NM 87185-1189, USA.

 ©2020 American Physical Society

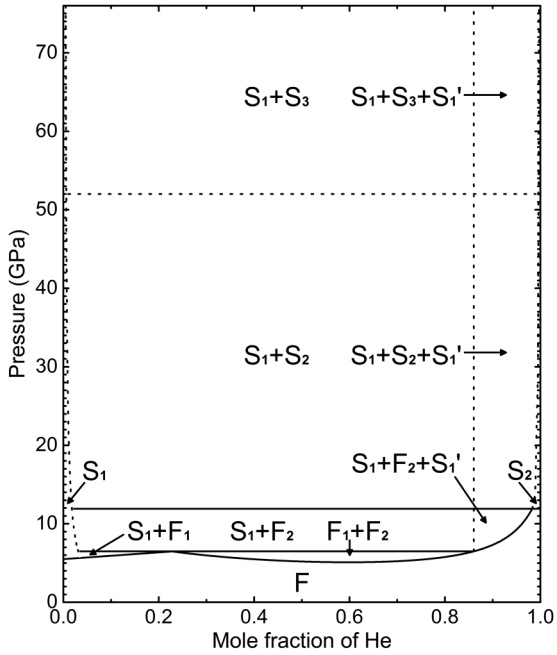

FIG. 1. Binary phase diagram of H_2-He, reproduced from Ref. [22]. F_1, F_2, S_1, and S_2 signify H_2-rich fluid, He-rich fluid, H_2-rich solid, and He-rich solid, respectively. S_1' and S_3 signify H_2-rich solid grown in He-rich fluid above the vertical dotted line, whereas S_3 refers to deformed S_2 (or a potential new structure) above 52 GPa or the horizontal dotted line.

account the interactions between H_2 and He [16]. However, recent first-principles calculations by Vorberger *et al.* [17] have predicted that under the influence of He presence, H_2 bonds become shortened and stronger, which leads to an enhanced stability of H_2 in H_2-He mixtures compared to that in pure H_2 in the pressure range of 10–120 GPa. McMahon *et al.* [18] have also pointed out that the existing EOS models for H_2-He mixtures are still based on those of pure H_2 and He with a linear mixing approximation, and in order to calculate an accurate EOS for planetary modeling, the assumption should be removed. Furthermore, the low-temperature studies on H_2-He mixtures have shown the formation of an interesting He-rich cluster surrounding H_2 impurities (or H_2@He) through van der Waals forces [19,20], underscoring the significance of defect-induced miscibility/chemistry in these quantum solid mixtures even at 0 K [21].

Recently, we have studied H_2-He mixtures to 75 GPa at room temperature using Raman spectroscopy [22]. The main results were as follows: (i) a binary phase diagram of H_2-He to 75 GPa, as reproduced in Fig. 1; (ii) a significant level of mixing between H_2 and He, giving rise to strongly blueshifted H_2 vibrons in both He-rich liquid and solid; (iii) a possible structural phase transition in He at ∼52 GPa, where the blueshifted H_2 vibrons abruptly disappear in the H_2-incorporated He lattice; and (iv) an interesting vibron at 2330 cm^{-1}, suggesting a strong chemical association between H_2 and He. Subsequent studies by Turnbull *et al.* [23], however, have challenged those findings in Ref. [22] and suggested no spectral evidence for the miscibility and chemical association between H_2 and He up to 250 GPa at 300 K. Interestingly, Loubeyre *et al.* [24] have also shown highly blueshifted H_2 vibrons in He-rich liquid below 12 GPa, indicating the presence of H_2 in liquid He.

Extending the previous Raman study, we have carried out high-pressure XRD studies to understand compression behaviors and structure changes of H_2 and He in H_2-He mixtures. We emphasize that the primary objective of the present paper is to obtain the EOS of H_2-He mixtures over an extended pressure range and examine any pressure-induced structural change in these mixtures—not to address the controversy in the previous Raman data [22,23]. This is simply because the present powder x-ray diffraction data of H_2-He are not suitable to probe the structural origin of the Raman band that comes from a local structure.

The XRD experiments were performed at five different compositions: 1:99 (or 99%), 1:9 (90%), 1:1 (50%), 9:1 (10%), and 99:1 (1%) in H_2:He (He) mole fractions, and in pure H_2 and pure He for comparison. The diffraction results show that both H_2 and He in the H_2-He mixtures remain as hcp to the maximum pressure studied 160 GPa, yet they develop a substantial level of lattice distortion in the (100) plane, most profound in He-rich solids and below 66 GPa. The diffraction data also reveal the evidence of structural deformation in hcp lattices of H_2 and He in the mixtures, substantially greater than those in pure H_2 and He, resulting in the increase of compressibility upon increasing the mixing ratio and with the maximum value at the 1:1 mixture. Also, the PV compression data measured in H_2-rich and He-rich solids to 160 GPa deviate from those of pure H_2 and pure He, providing new constraints for the development of the EOS models of H_2-He mixtures for Giant planets.

II. EXPERIMENTAL METHODS

Ultrahigh purity hydrogen (99.999%) and helium (99.999%) gases were used to prepare the pure and mixture samples. The gas mixture samples were compressed to ∼0.2 GPa and loaded into the high-pressure sample chamber in diamond anvil cells (DACs), using a home-built high-pressure gas loading (HPGL) system. Prior to mixing the gaseous samples, all high-pressure lines and high-pressure valves, a two-stage compressor, and lecture bottles in the HPGL system were vacuumed and flushed very carefully with either H_2 or He multiple times in order to minimize any possible impurity contamination from the air and so on. The sample chamber in DACs was created with preindented (from 200 μm down to 20–50 μm thick) rhenium gaskets with holes (80–160 μm in diameter) drilled at the center by an electrical discharge machine (EDM) and with two opposing diamond anvils (1/3-carat, type Ia) with the central flat diameters in 300 μm (unbeveled) and 180 and 100 μm (beveled at 8° from 300 μm in diameter). One small ruby ball (∼5 μm in diameter) was loaded prior to the sample loading for the pressure calibration [25] to ∼70 GPa, above which the Raman edge of diamond anvil [26] was used.

All high-pressure experiments were performed at room temperature with a large number of samples (over a dozen)

with five different compositions of 99%, 90%, 50%, 10%, and 1% in He mole fraction, as well as pure H_2 and pure He, for comparison. Hydrogen was assumed to be a 3:1 ortho-para mixture at ambient temperature. Powder x-ray diffraction experiments were carried out using microfocused (less than $10\,\mu\text{m} \times 10\,\mu\text{m}$) third-generation synchrotron x-rays; at the BL10XU ($\lambda = 0.4128$ Å) at SPring-8 in Japan, P02.2 ($\lambda = 0.4824$ Å) at PETRA III in Germany, and the HPCAT ($\lambda = 0.4066$ Å) at APS in the US X-ray diffractions were recorded over a relatively large 2θ range between 3° and 40° using high spatial resolution 2D pixel detectors such as a Rigaku image plate at BL10XU, a PE XRD1621 at P02.2, and a MARCCD at HPCAT. The measured 2D diffraction images were then converted into 1D diffraction angle-resolved diffraction patterns using on-line DIOPTAS software [27].

III. RESULTS

Because of a partial miscibility between H_2 and He in both solids and liquids [22], it is difficult to determine the exact composition of H_2-He mixtures at different pressures. Thus, the composition of H_2-He should be considered as its nominal value (i.e., the composition at loading) and, therefore, we will present the results according to the compression behaviors of fluids (in Sec. III A), H_2-rich solid mixtures (Sec. III B), and He-rich solid mixtures (Sec. III C). Furthermore, while showing a lesser degree of preferred orientation in the mixtures than in pure H_2 or pure He, the mixtures still exhibit a substantial level of preferred orientation. Thus, the measured intensities of diffraction lines are not ideal. Nevertheless, we should note that the measured peak positions, spectral shapes, and, to an extent, relative intensities of observed diffraction lines are consistent over the same pressure ranges among different samples.

A. Solidification and mixing of H_2-He

To understand XRD patterns of H_2-He mixtures, it is important to consider the mixing behavior between H_2 and He at different pressures and composition rates, reflected on visual appearance, spectral/diffraction changes, and binary phase diagram in Fig. 1 [22,28]. At ambient temperatures, H_2 and He are completely miscible at relatively low pressures (below ~3 GPa), forming a homogeneous fluid (F), regardless of the composition. Interestingly, in the intermediate composition between ~20% and 85% He, homogeneous fluid separates into two immiscible fluids, H_2-rich F_1 and He-rich F_2, which coexist together with F_1 between 3 and 5.5 GPa, and above 5.5 GPa it transforms into a mixture of H_2-rich solid S_1 and F_1 or F_2 depending on the composition. Note that pure H_2 and He solidify at 5.5 and 12 GPa, respectively.

Solidifications of H_2-rich F_1 and He-rich F_2 fluids occur at substantially higher pressures than pure H_2 and pure He. For example, He-rich fluids (with 99 and 90% He) remain as homogeneous fluids to ~12 and 7 GPa, respectively, where they solidify to He-rich solid S_2. Such a retarded solidification of H_2 well above 5.5 GPa in fluid He results in the appearance of metastable H_2-rich solids (S_1') in He-rich fluids. Similarly, H_2-rich fluids (with 99% and 90% H_2) are separated into S_1 and F_2 and then S_1 and S_2 at even higher than 12 GPa. The first appearance of powder diffraction of solid H_2 in S_1 (or He in S_2) is at ~15–30 GPa. These results indicate strongly retarded solidification of the host lattice by the presence of guest molecules in both He-rich and H_2-rich mixtures.

It is important to note that the solidification in H_2-He is apparent at the onset of transition in visual appearance and Raman spectra, but it is difficult to discern in the x-ray diffraction. Instead, H_2-He mixtures regardless of the composition start to exhibit the x-ray diffraction pattern only after sufficiently surpassing the solidification, that is, at ~15–20 GPa. This is likely due to the diffusive nature of He and H_2 even after the solidification, resulting in a disordered lattice. In comparison, pure He and H_2 form more ordered crystals, as all published data below 30 GPa [6,7] are primarily from single-crystal x-ray diffractions. The diffusive nature of H_2 and He in the mixture, on the other hand, seems consistent with the miscibility of H_2-He previously suggested [22] and why H_2-He forms a better polycrystalline sample above ~20–30 GPa. The powder diffraction patterns of H_2-He mixtures remain observable to at least 160 GPa (see Fig. S1 [29]), although the diffraction data in Fig. 2 are shown to 129 GPa to signify the data taken from the same batch of sample.

B. Compression behavior of H_2 in H_2-rich solid

Figure 2 shows the diffraction patterns of hcp H_2 in three H_2-rich mixtures with the H_2 mole fractions of (a) 99%, (b) 90%, and (c) 50%, shown together with those of pure H_2 in the inset of Fig. 2(a) for comparison. Clearly, H_2 and He remain as hcp to the maximum pressure studied. On the other hand, several differences are notable in the figure. First, the diffraction patterns are composed primarily of (100) and (101) reflections. The absence of (002) indicates that the crystal is preferably oriented along the c-axis parallel to the incident x-rays or the primary stress direction in DAC [10]. Second, it is also important to note that the (100) peaks in all mixtures are relatively weak with respect to the (101), becoming diminishingly weak especially in the 50% mixture. Therefore, it is conceivable that the weak (100) intensity is related to the lattice distortion introduced by a substantial amount of He incorporation. It is also interesting to note that the intensities of hcp H_2 diffraction lines (red lines) are stronger than those of hcp He (gray lines) in the 50% mixtures [Fig. 2(c)], which is counterintuitive knowing that the atomic scattering factor is higher or at least similar in He than that of H_2. Finally, it is remarkable that the diffraction patterns of H_2 are observed to pressures well above 100 GPa in the mixtures, despite the well-known fact that H_2 has extremely low x-ray intensity.

The compression curves of H_2-He mixtures are plotted in Fig. 3: (a) the specific V and V/V_0 in the inset and (b) the c/c_0, a/a_0, and c/a in the inset, all as a function of pressure. The PV curves of H_2-He mixtures are in good agreement with that of pure H_2 at low pressures [8], but they begin to deviate above ~79 GPa. Similarly, the a/a_0 and c/c_0, as well as the c/a in Fig. 3(b) show some differences between the present and previous data above ~70 GPa. Thus, the different compression behavior appears to be related to the lattice distortion of H_2-He.

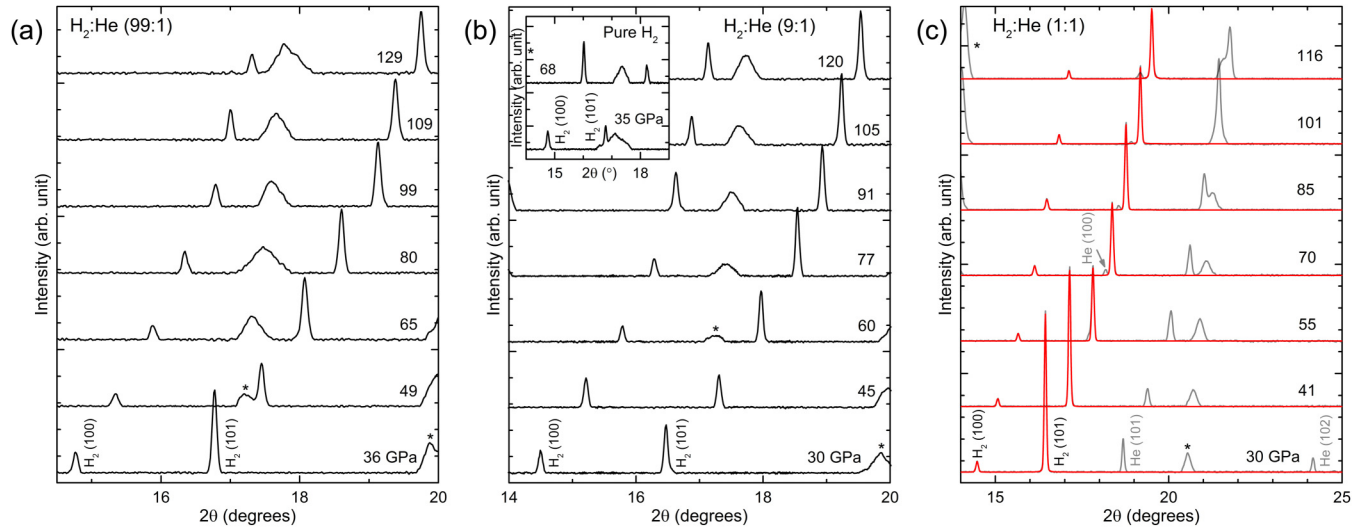

FIG. 2. Representative high-pressure XRD patterns of hcp H_2 in H_2-He mixtures with three compositions: (a) 99%, (b) 90%, and (c) 50% H_2 mole fractions at room temperature. The inset in (b) shows the selected XRD patterns of pure H_2 under high pressures for comparison. Note that the diffraction patterns of H_2 in the 50% mixture are colored in red in (c), whereas those of He are shown in gray. Bragg peaks from Re gaskets are marked with * symbols.

The PV compression data have been examined based on the Vinet equation of state (EOS) fits using a fixed $V_0 = 84.464$ Å^3/unit cell [8]. Results of the EOS fits are summarized in Table I. Importantly, the bulk modulus B_0 value of mixtures shown in the Fig. 3(a) inset decreases as the He concentration increases. For example, the B_0 of H_2 decreases from 0.113 GPa in the 99% H_2 mixtures to 0.080 GPa in the 50% H_2 mixtures. The softening of the H_2 lattice with

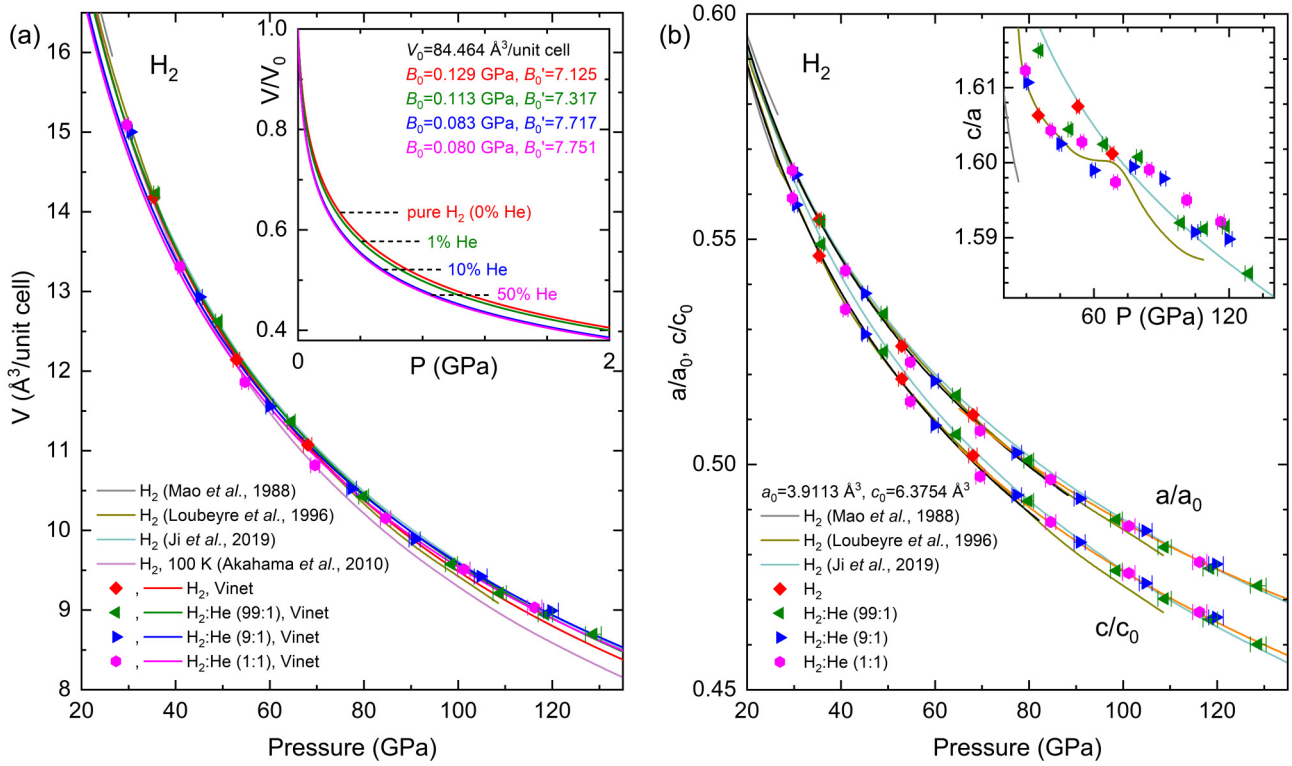

FIG. 3. The 300 K PV isotherm of hcp H_2 in H_2-rich H_2-He mixtures along with pure H_2, plotted in terms of (a) unit cell volume and (b) relative a and c lattice parameters as a function of pressure. Solid lines in red, green, blue, and magenta in (a) represent the Vinet EOS fits to the present data comparing with pure H_2 (other solid lines) from Refs. [6,8–10]. Black and orange lines in (b) are drawn as guides to the eye. Error bars for the volume are within the symbol sizes. Insets in (a) and (b) show a magnified view of the 0–2 GPa region of relative volume and pressure-dependent c/a ratio, respectively.

TABLE I. EOS parameters of hcp H_2 and He and in H_2-He mixtures in comparison with those of the present pure H_2 and He and those previously reported for pure H_2 and He. The values in parentheses are the uncertainties in B_0 and B_0' associated with the EOS fits.

Sample	EOS	V_0(Å^3/unit cell)	B_0 (GPa)	B_0' (no unit)	P range (GPa)	Reference
			H_2			
H_2:He (99:1)	Vinet	84.464	0.113 (± 0.016)	7.317 (± 0.176)	36–129	This work
H_2:He (9:1)	Vinet	84.464	0.083 (± 0.015)	7.717 (± 0.238)	30–120	This work
H_2:He (1:1)	Vinet	84.464	0.080 (± 0.015)	7.751 (± 0.240)	30–116	This work
H_2	Vinet	84.464	0.129 (± 0.024)	7.125 (± 0.258)	35–68	This work
H_2	Vinet	84.464	0.162	6.813	7–109	[8]
H_2	Vinet	84.495	0.110	7.367	20–254	[9]
H_2, 100 K	Vinet	76.384	0.275	0.639	20–183	[10]
			He			
H_2:He (1:99)	Vinet	45.565	0.206 (± 0.024)	7.496 (± 0.177)	18–73	This work
H_2:He (1:9)	Vinet	45.565	0.141 (± 0.010)	8.115 (± 0.097)	17–161	This work
H_2:He (1:1)	Vinet	45.565	0.160 (± 0.029)	7.908 (± 0.263)	16–116	This work
He	Vinet	45.565	0.266 (± 0.037)	7.100 (± 0.214)	30–67	This work
He	Vinet	45.565	0.225	7.35	12–58	[11]
He	Vinet	62.16	0.039	8.63	12–75	[30]

an increase of He is consistent with the He-induced lattice distortion observed in the (100) diffraction plane, especially in Fig. 2(c).

C. Compression behavior of He in He-rich solid

Figure 4 shows the diffraction patterns of hcp He in He-rich mixtures with the He mole fraction of (a) 99%, (b) 90%, and (c) 50%, together with those of pure He in the Fig. 4(a) inset and a 2D diffraction image of 90% He at 161 GPa in the Fig. 4(b) inset. The 99% He mixture shows relatively strong reflections including (100), (002), (101), (102), and (110) with respect to the 90% or 50% mixtures, clearly indicating a lesser degree of preferred crystal orientation in the 99% mixture. In pure He, only (100) and (101) are measurable [see Fig. 2(a), inset]. This result is likely due to a small amount of solid H_2 dispersed in fluid He perturbing the crystallization of He above 12 GPa. In fact, it is analogous to the previous result that He forms van der Waals clusters centered around H_2 impurities at low temperatures [19,20]. Interestingly, the (100) in 90% He in Fig. 4(b) becomes significantly weakened with increasing pressure, while the (101) stands out as an intense peak with almost no change in intensity to 124 GPa. The 50% He behaves similarly to the 90%, underscoring the increase of lattice distortion in the hcp basal plane (001) with increasing H_2 as reflected in the distorted (100) peak (i.e., basal plane defects).

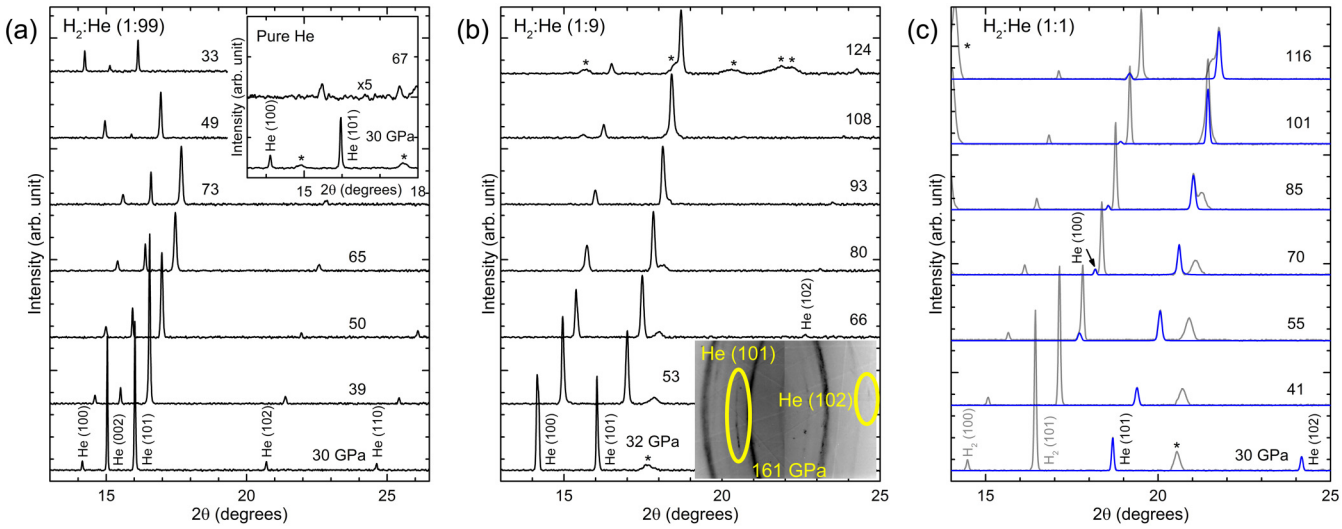

FIG. 4. Selected high-pressure XRD patterns of hcp He in H_2-He mixtures with three compositions of (a) 99%, (b) 90%, and (c) 50% in He mole fractions at room temperature. Insets in (a) and (b) represent high-pressure XRD patterns of pure He and the diffraction image plate of hcp He in a 1:9 mixture at 161 GPa (the highest pressure reached; also see Fig. S1 [29]), respectively. The 99% He mixture shows the most diffraction lines, including (100), (002), (101), (102), and (110), in comparison with other concentrations. Solid blue lines in (c) remark Bragg peaks from hcp He in a 1:1 mixture to distinguish other contributions (gray solid lines) such as hcp H_2 and the Re gasket. The contribution from the Re gasket is marked with a * symbol.

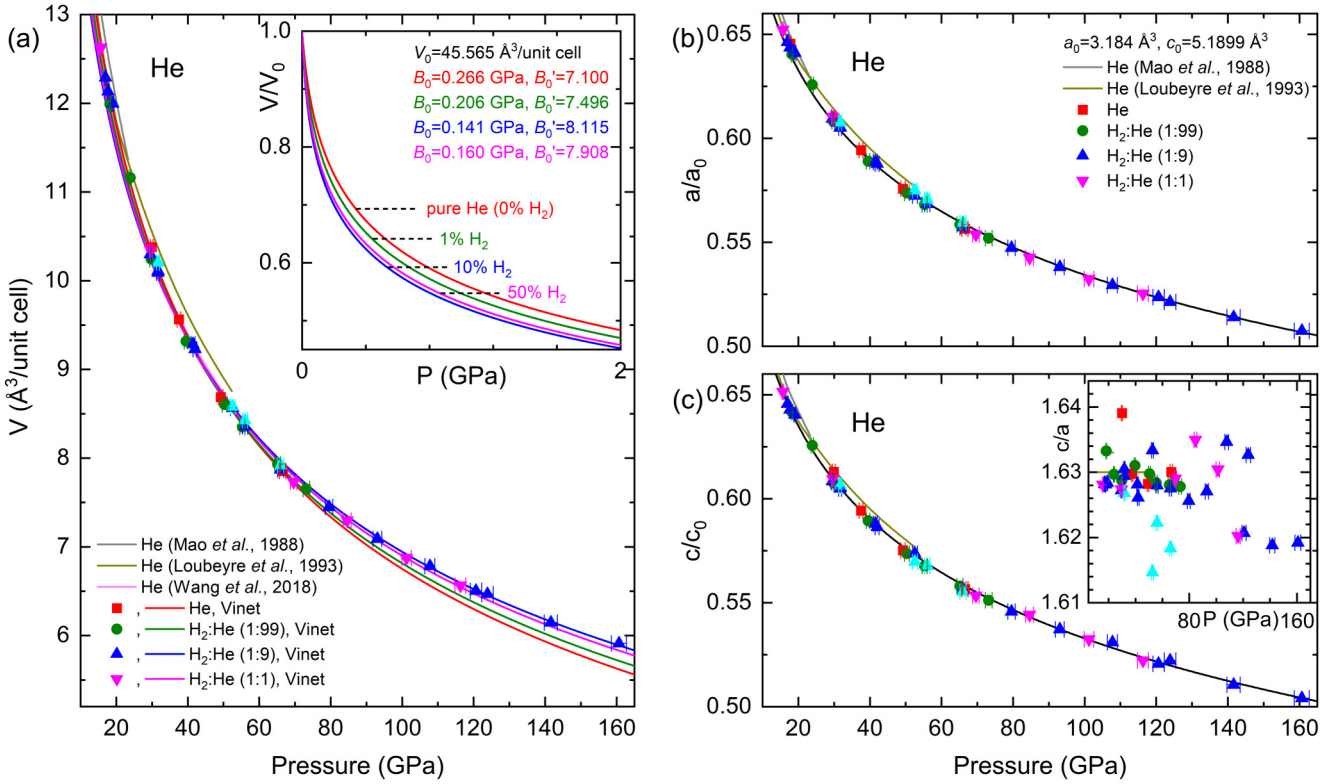

FIG. 5. The 300 K PV-isotherm of hcp He in He-rich H_2-He mixtures along with pure He, plotted in terms of (a) unit-cell volume, (b) relative a lattice parameter, and (c) relative c lattice parameter, as a function of pressure. Solid lines in red, green, blue, and magenta in (a) represent the Vinet EOS fits to the present data compared with pure He (other solid lines) from Refs. [7,11,30]. The distorted lattice of hcp He in a 90% He-rich mixture is denoted by a light blue triangle symbol. Black lines in (b) and (c) are drawn as guides to the eye. Error bars for the volume are within the symbol sizes. Insets in (a) and (c) show a magnified view of the 0–2 GPa region of relative volume and pressure-dependent c/a ratio, respectively.

The compression curves of He-rich mixtures are plotted in Fig. 5: (a) the specific V and V/V_0 in the inset, (b) the a/a_0, and (c) the c/c_0 and the c/a in the inset, all as a function of pressure. Note that the present PV curve of pure He is significantly different from that of the previous data by Loubeyre *et al.* [11], but agrees well with the more recent one by Wang *et al.* [30]. The difference is also apparent in a/a_0, c/c_0, and c/a. For example, the c/a ratio in the Fig. 5(c) inset strongly fluctuates when the concentration of H_2 increases in the mixtures, underscoring the H_2-induced lattice distortion of hcp He. Interestingly, the c/a ratio of the distorted He lattice [light blue triangles in the Fig. 4(c) inset; see also Fig. 5] is substantially smaller than those of 99%, 90%, and 50% He-rich mixtures, indicating the incorporation of H_2 substituting He within the (100) plane, rather than the interstitial between the (100).

The pressure-volume compression data have been examined based on the Vinet EOS fits with a fixed $V_0 = 45.565\,\text{Å}^3/\text{unit cell}$ [11]. The results are summarized in Table I. The B_0 value of He in He-rich mixtures decreases from 0.206 to 0.160 GPa, as the H_2 concentration increases from 1% to 50%, highlighting the H_2-induced lattice distortion and softening of He-rich mixtures.

IV. DISCUSSION

The present diffraction data indicate that both H_2 and He in the H_2-He mixture remain as hcp to the maximum pressure applied, 160 GPa. Nevertheless, it is evident that the hcp lattice develops a substantial level of distortion in the (100) plane, especially profound in He-rich solids and below 66 GPa. The diffraction lines become notably distorted and asymmetric shapes, for example, in 90% He-rich solids between 32 and 66 GPa (Fig. 6). In addition, the spectral shapes, peak position, and intensities of observed He diffraction lines are greatly different depending on the specific location of the He-rich region. The asymmetric diffraction lines come from the He-rich region having large lattice distortion, while the symmetric diffraction lines come from another He-rich region with significantly low or without distortion. The distinct lattice distortion reflects a heterogeneous nature of He-rich solid, arising from H_2 inclusions in the hcp He host lattice. Interestingly, above 66 GPa the distortion in the diffraction lines disappears, despite collecting the diffraction at the same spot.

It appears that the lattice distortion accompanies the softening of both H_2-rich and He-rich solids more than pure H_2 and He, respectively, by ~38% and 40% in B_0 values. The distortion becomes larger as the minor composition increases and maximizes at 50%. These results, the distortion in the (100) plane and the softening of the hcp lattice, clearly indicate some inclusions of H_2 into He-rich solid and He in H_2-rich solid of He-H_2 mixtures.

The observed miscibility between H_2 and He is not surprising, considering the diffusive nature of H_2 and He, even in

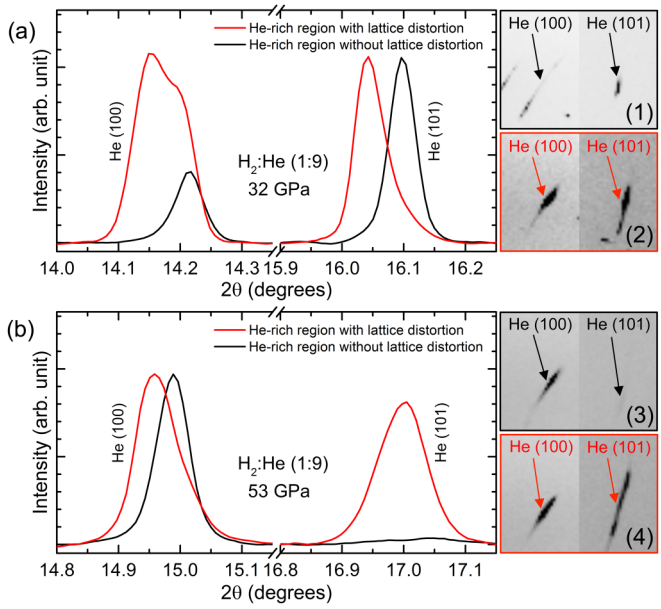

FIG. 6. The XRD patterns of the distorted lattice (denoted by solid red lines) of hcp He in 90% He-rich mixture compared with those of other sample areas without lattice distortion (solid black lines) at (a) 32 GPa and (b) 53 GPa, respectively. The corresponding diffraction images are also shown on the right to compare the distorted [red box, labeled as (2) and (4)] and undistorted [black box, labeled as (1) and (3)] diffraction images.

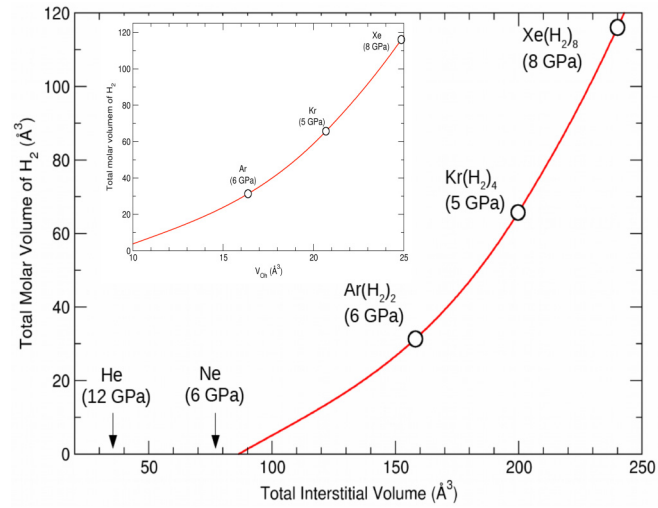

FIG. 7. H_2 molar volumes of noble-gas solid hydrides, $Xe(H_2)_8$, $Ar(H_2)_4$, and $Kr(H_2)_2$, plotted as a function of the interstitial volumes, illustrating an interstitial filled mixing of H_2 in Xe, Ar, and Kr, and maybe Ne—not in He. The specific volume of solid H_2 is larger than that of the largest octahedral interstitial site of hypothetical fcc He at 12 GPa. It is likely that the mixing of H_2-He occurs via a substitutional H_2 inclusion into the basal plane of hcp-He.

solids. In fact, the evidence is ample, including H_2 diffusion into metals, graphite, and ice [31,32], the formation of solid solutions such as H_2-rich S_1 and He-rich S_2 [22], the formation of He clusters surrounding H_2 solids [19,20], as well as the formation of novel van der Waals compounds such as $Ar(H_2)_2$ [33,34], $Kr(H_2)_4$ [35], and $Xe(H_2)_8$ [36] at high pressures. Apparently, a simple interstitial filled model can explain the formation of noble-gas solid hydrides rather well as illustrated in Fig. 7, which in turn suggests a diffusive mixing of fluid/solid H_2 into solid Ar/Kr/Xe. In this plot, the total interstitial volumes represent the summation of four octahedral (Oh) and eight tetrahedral (Td) interstitial volumes in fcc rare-gas solid structures at the observed transition pressures [33–36]. For comparison, He is also approximated as fcc because of a small difference in volume between hcp-He and fcc-He. Note that the calculated Oh volume of He or Ne (marked with an arrow) is smaller than the molar volume of H_2, underscoring a different mixing mechanism, especially in H_2-He mixtures. The specific volume of He is also bigger than the Oh volume of solid H_2; thus, it is unlikely for He to diffuse into the interstitial site of H_2.

We consider a substitutional mechanism similar to the formation of H_2@He clusters at low temperatures [19–21]; that is, liquid He initially captures or may even form a cluster surrounding H_2 upon the solidification at ∼5.5 GPa, which then transforms to a substitutionally disordered hcp-He lattice upon the solidification of He above ∼12 GPa. The observed disorder in the (100) plane is then consistent with the substitutional disorder in the hcp basal plane. The anomalous change in the c/a ratio at ∼60 GPa [see the insets of Figs. 2(b) and 4(c)], as well as the substantial decrease of the c/a especially in distorted He-rich solids also support this conjecture of H_2 inclusion in the He lattice.

The formation of He clusters around solid H_2 and the mixing of H_2-He are kinetic processes, which would depend on the loading of samples. This is particularly important, because H_2 and He solidify at very different pressures, 5.5 and 12 GPa, respectively. Therefore, it is possible that the apparent difference in the previous observations in H_2-He [22,23] may reflect the difference in kinetics associated with H_2 crystallization in fluid He.

The present diffraction data cannot completely rule out the possibility that there could be a subtle structural change above 50–60 GPa, including the formation of a stacking disordered hcp from *ABAB* to *ABAB*′, where *B* and *B*′ differ by a degree of disorder in H_2 inclusions, as well as to *ABCABC*, where *B* and *C* signify H_2-rich and He-rich layers. These structural changes can be considered in terms of a configurational order-disorder transition in substitutionally disordered H_2-He sublattices, which may accompany only a subtle diffraction change difficult to discern in the present data from a preferably oriented sample and a limited 2θ angle.

It is remarkable that the diffraction patterns in H_2 and He in the mixtures remain strong at pressures well above 100 GPa and ambient temperatures. This is in contrast to those of pure H_2 and He. We attribute the apparent intensity enhancement in the mixture to the formation of better polycrystalline samples in the mixtures. Nevertheless, the diffraction lines of He-rich mixtures seem less preferably oriented, as the presence of H_2 disturbs the crystalline ordering of fluid He.

Finally, the present compressional data of H_2 and He in their mixtures deviate from those of pure H_2 and He. Based on the Vinet EOS fits, we found that the bulk modulus B_0 value in the mixtures decreases with the increase of H_2 (or He) concentration at the rate of $-0.007\text{GPa}/10\%\text{H}_2$ (or

−0.013 GPa/10%He). The decrease of B_0 which minimizes at 1:1 mixture seems to reflect the mixing of H_2 and He and subsequent lattice distortion and softening. The present EOS results of H_2-He mixtures provide new constraints for the giant planetary models, since they are more relevant than those of pure H_2 and He.

ACKNOWLEDGMENTS

The present study has been performed in support of the DOE-NNSA (DE-NA0003342), NSF (DMR 1701360), and ARO (W911NF-17-1-0468). The x-ray work has been performed at PETRA III and beamline P02.2 in Germany, 10XU/SPring-8 in Japan, and the HPCAT/APS in the US. We acknowledge DESY (Hamburg, Germany), a member of the Helmholtz Association HGF, for the provision of experimental facilities. HPCAT operations are supported by DOE-NNSA's Office of Experimental Sciences. The Advanced Photon Source is a US Department of Energy (DOE) Office of Science User Facility operated for the DOE Office of Science by Argonne National Laboratory under Contract No. DE-AC02-06CH11357.

[1] E. Polturak and N. Gov, Contemp. Phys. **44**, 145 (2003).
[2] E. Babaev, A. Sudbo, and N. W. Ashcroft, Phys. Rev. Lett. **95**, 105301 (2005).
[3] H. E. Suess and H. C. Urey, Rev. Mod. Phys. **28**, 53 (1956).
[4] S. K. Atreya, M. H. Wong, T. C. Owen, P. R. Mahaffy, H. B. Niemann, I. de Pater, P. Drossart, and Th. Encrenaz, Planet. Space Sci. **47**, 1243 (1999).
[5] T. Guillot, Science **286**, 72 (1999).
[6] H. K. Mao, A. P. Jephcoat, R. J. Hemley, L. W. Finger, C. S. Zha, R. M. Hazen, and D. E. Cox, Science **239**, 1131 (1988).
[7] H. K. Mao, R. J. Hemley, Y. Wu, A. P. Jephcoat, L. W. Finger, C. S. Zha, and W. A. Bassett, Phys. Rev. Lett. **60**, 2649 (1988).
[8] P. Loubeyre, R. Le Toullec, D. Hausermann, M. Hanfland, R. J. Hemley, H. K. Mao, and L. W. Finger, Nature (London) **383**, 702 (1996).
[9] C. Ji, B. Li, W. Liu, J. S. Smith, A. Majumdar, W. Luo, R. Ahuja, J. Shu, J. Wang, S. Sinogeikin, Y. Meng, V. B. Prakapenka, E. Greenberg, R. Xu, X. Huang, W. Yang, G. Shen, W. L. Mao, and H.-K. Mao, Nature (London) **573**, 558 (2019).
[10] Y. Akahama, M. Nishimura, H. Kawamura, N. Hirao, Y. Ohishi, and K. Takemura, Phys. Rev. B **82**, 060101(R) (2010).
[11] P. Loubeyre, R. Le Toullec, J. P. Pinceaux, H. K. Mao, J. Hu, and R. J. Hemley, Phys. Rev. Lett. **71**, 2272 (1993).
[12] B. L. Holian, W. D. Gwinn, A. C. Luntz, and B. J. Alder, J. Chem. Phys. **59**, 5444 (1973).
[13] Y. J. Gu, Q. F. Chen, L. C. Cai, Z. Y. Chen, J. Zheng, and F. Q. Jing, J. Chem. Phys. **130**, 184506 (2009).
[14] M. A. Morales, E. Schwegler, D. Ceperley, C. Pierleoni, S. Hamel, and K. Caspersen, Proc. Natl. Acad. Sci. USA **106**, 1324 (2009).
[15] M. A. Morales, S. Hamel, K. Caspersen, and E. Schwegler, Phys. Rev. B **87**, 174105 (2013).
[16] G. Chabrier, S. Mazevet, and F. Soubiran, Astrophys. J. **872**, 51 (2019).
[17] J. Vorberger, I. Tamblyn, B. Militzer, and S. A. Bonev, Phys. Rev. B **75**, 024206 (2007).
[18] J. M. McMahon, M. A. Morales, C. Pierleoni, and D. M. Ceperley, Rev. Mod. Phys **84**, 1607 (2012).
[19] S. I. Kiselev, V. V. Khmelenko, and D. M. Lee, Phys. Rev. Lett. **89**, 175301 (2002).
[20] E. B. Gordon, Low Temp. Phys. **30**, 756 (2004).
[21] A. F. Andreev and L. M. Lifshitz, J. Exp. Theor. Phys. **29**, 1107 (1969).
[22] J. Lim and C.-S. Yoo, Phys. Rev. Lett. **120**, 165301 (2018).
[23] R. Turnbull, M.-E. Donnelly, M. Wang, M. Peña-Alvarez, C. Ji, P. Dalladay-Simpson, H. K. Mao, E. Gregoryanz, and R. T. Howie, Phys. Rev. Lett. **121**, 195702 (2018).
[24] P. Loubeyre, R. Le Toullec, and J. P. Pinceaux, Phys. Rev. B **36**, 3723 (1987).
[25] H. K. Mao, J. Xu, and P. M. Bell, J. Geophys. Res. **91**, 4673 (1986).
[26] Y. Akahama and H. Kawamura, J. Appl. Phys. **100**, 043516 (2006).
[27] C. Prescher and V. B. Prakapenka, High Press. Res. **35**, 223 (2015).
[28] P. Loubeyre, R. Le Toullec, and J. P. Pinceaux, J. Phys. Condens. Matter **3**, 3183 (1991).
[29] See Supplemental Material at http://link.aps.org/supplemental/10.1103/PhysRevB.101.224103 for the x-ray diffraction pattern of hcp He in a 1:9 H_2-He mixture at 161 GPa (Fig. S1).
[30] Y. Wang, X. Zhang, S. Jiang, Z. M. Geballe, T. Pakornchote, M. Somayazulu, V. Prakapenka, E. Greenberg, and A. F. Goncharov, J. Chem. Phys. **150**, 114504 (2019).
[31] J. K. Lim and C.-S. Yoo, Appl. Phys. Lett. **109**, 051905 (2016).
[32] G. M. Borstad and C.-S. Yoo, J. Chem. Phys. **135**, 174508 (2011).
[33] P. Loubeyre, R. Letoullec, and J.-P. Pinceaux, Phys. Rev. Lett. **72**, 1360 (1994).
[34] C. Ji, A. F. Goncharov, V. Shukla, N. K. Jena, D. Popov, B. Li, J. Wang, Y. Meng, V. B. Prakapenka, J. S. Smith, R. Ahuja, W. Yang, and H.-K. Mao, Proc. Natl. Acad. Sci. USA **114**, 3596 (2017).
[35] A. K. Kleppe, M. Amboage, and A. P. Jephcoat, Sci. Rep. **4**, 4989 (2014).
[36] M. Somayazulu, P. Dera, A. F. Goncharov, S. A. Gramsch, P. Liermann, W. Yang, Z. Liu, H.-K. Mao, and R. J. Hemley, Nat. Chem. **2**, 50 (2010).